Modulation-agnostic single-shot estimation of quantum measurement confidence

M. V. Jabir,* N. Fajar R. Annafianto, and A. Battou
National Institute of Standards and Technology, Gaithersburg, Maryland 20899, USA

I. A. Burenkov
National Institute of Standards and Technology, Gaithersburg, Maryland 20899, USA
and Joint Quantum Institute, University of Maryland, College Park, Maryland 20742, USA

Sergey V. Polyakov
National Institute of Standards and Technology, Gaithersburg, Maryland 20899, USA
and Department of Physics, University of Maryland, College Park, Maryland 20742, USA

(Received 31 July 2023; accepted 9 October 2023; published 2 November 2023)

We experimentally explore single-shot state identification using long alphabets of states and employing different modulation schemes. We use time-resolved quantum measurement and Bayesian inference to identify the input state and demonstrate the advantage of this single-shot measurement over classical state identification. For each single-shot measurement, we estimate the confidence of state identification based on the quantum measurement and demonstrate the physical significance of confidence estimates. Particularly, we show that a set of confidence values correctly represents the probabilities of successful state identification for a given experimental outcome. We investigate the alphabets of coherent states with different modulations and show that confidence estimates yield the reliability of each act of measurement independently of the modulation used.

DOI: 10.1103/PhysRevA.108.052203

I. INTRODUCTION

The state of a physical system can be revealed to an observer through measurement. However, in quantum mechanics, generally speaking, the complete knowledge of a physical state cannot be obtained through measurements. That is, it is impossible to know the state of the quantum system that belongs to the nonorthogonal set with full certainty. A class of problems in quantum measurement, known as state-identification problems, is finding the particular unknown state of a system that can be in one of the states from a known set by measuring just one copy. Such state identification, generally speaking, cannot be perfect due to inherent uncertainties of the quantum measurement: only partial information about the measured state can be obtained [1,2]. Quantifying the amount of information and accuracy that can be obtained is important. Certain figures of merit can be identified, and the measurement can be optimized accordingly [3]. One such figure of merit is the probability of incorrect identification. The fundamental limit of measurement accuracy set by the quantum theory that leads to errors in identifying one of the physical states is known as the Helstrom bound [4]. Classically, the shot-noise limit sets the error bound. It has been shown that quantum measurements can significantly improve the accuracy of state identification compared to classical measurements [5–10]. However, the probability of incorrect identification and most other metrics considered in the literature use averages over a large ensemble of state identifications to arrive at a quantitative result [11–13]. Yet because quantum measurement outcomes are probabilistic, every individual measurement is unique and can be either more or less trustworthy than the statistical average.

Weak coherent states are advantageous for practical applications due to their ease of generation and manipulation. Discriminating between weak coherent states is closely related to classical communication. Recently, adaptive coherent-state displacement strategies were successfully used to demonstrate error rates that are below the (classical) shot-noise limit [11–25]. Even though adaptive displacement measurement strategies yield probabilistic outcomes for each individual act of measurement, most of the prior literature uses large ensembles to arrive at estimates. A recent report did consider individual measurement outcomes [26]. Particularly, this work confirmed that the set of posterior probabilities that the input is in a particular state from the set is the best information about the input that can be known after a single measurement. This set of probabilities, called confidences, can be understood as the estimate of the reliability of a given act of measurement. However, only one alphabet set has been studied, the quadrature phase-shift keying (QPSK). It is crucial to extend the testing of single-shot confidence estimation to multiple modulation schemes and use a larger number of states to showcase the universal character of this concept and provide experimental evidence of its robustness and versatility. The implications of this research are threefold. Fundamentally, the physical relevance of confidence sets needs to be experimentally established. Practically, if, indeed, a confidence

*jabirmv081@gmail.com

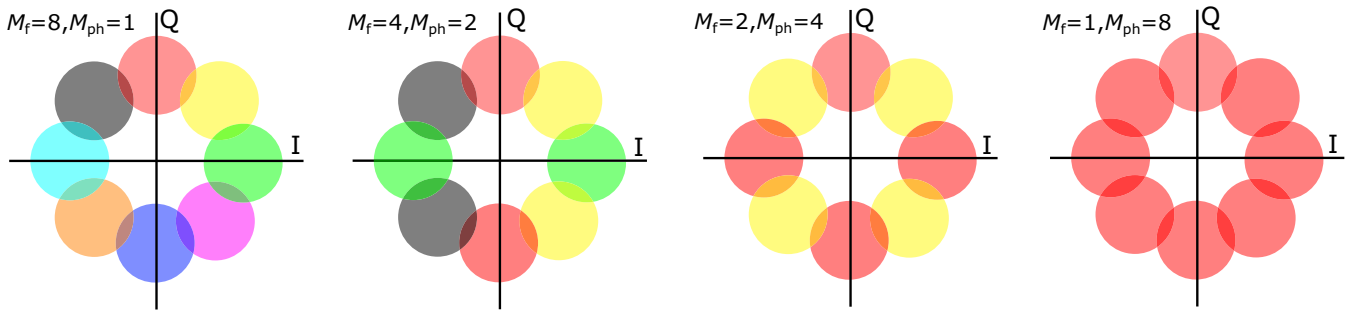

FIG. 1. Constellation diagrams of modulation schemes with $M = 8$ coherent states that are used in this work. (a) $M_f = 8$, $M_{\rm ph} = 1$, where all states are encoded in eight different frequencies, known as CFSK. (b) $M_f = 4$, $M_{\rm ph} = 2$, where states are encoded in four different frequencies and two phases per frequency. (c) $M_f = 2$, $M_{\rm ph} = 4$, where states are encoded in two frequencies and four phases per frequency. (d) $M_f = 1$, $M_{\rm ph} = 8$, where all states are encoded in phases with one frequency, known as PSK.

set is a more accurate description of our knowledge about the input state after the measurement, this information may be leveraged in practical devices such as telecommunication receivers, e.g., for the most efficient error correction (cf. [27]). Fundamentally, this research tests the quantum Bayesianist's view on quantum measurement [28].

Different degrees of freedom can be utilized to modulate weak coherent states. Phase and frequency are the two essential degrees of freedom that are especially convenient for encoding digital information in optical communication. Here, we use sets, or alphabets of $M = 8$ coherent states that are modulated in phase [phase-shift keying (PSK)], frequency [coherent frequency-shift keying (CFSK)], or both phase and frequency [hybrid frequency-phase-shift keying (HFPSK)]. Here, PSK provides maximal bandwidth efficiency in the channel at the expense of energy, CFSK provides energy efficiency at the expense of bandwidth, and HFPSK optimizes both energy and bandwidth use in the communication channel [25,29]. We use the same experimental setup and take advantage of the continuous quantum measurement. In our measurement device, the optimal choice of adaptive signals and the probability of identification error vary per modulation scheme, as do the confidence estimates. In this work, we obtain the confidence estimates of each act of measurement independently and compare those estimates to the observed probability of error using a long set of measurements and ensemble averages. We find the direct correspondence between the confidence values (Bayesian posterior probability estimates) and "intrinsic" (frequentist) probabilities obtained experimentally. Our results demonstrate the direct relationship between the two probabilities, which enables the practical use of Bayesian estimates, e.g., for quantum-enabled error correction.

II. RESULTS AND DISCUSSION

A. Modulation methods

We use different modulation schemes with eight states (in other words, the alphabet length is $M = 8$). Particularly, we use a modulation-scheme family that is common to optical communication. The states in the modulation scheme are encoded in frequency and/or phase. The coherent states can be written as $\{|\alpha(\omega_i, \theta_{ij})\rangle\}$. For each frequency $\omega_i = \omega_0 + (i-1)\Delta\omega$, $i \in 1, \ldots, M_{\rm f}$, the initial phase is $\theta_{ij} = (i-1)\Delta\theta_{\rm f} + (j-1)\Delta\theta_{\rm ph}$, where $j \in 1, \ldots, M_{\rm ph}$ and $\Delta\theta_{\rm ph} = 2\pi/M_{\rm ph}$, such that $M = M_{\rm f} \times M_{\rm ph}$. Note that we are interested in nonorthogonal states, so that $T\Delta\omega < 2\pi$, where T is the duration of our flat-top laser pulses. For each M, several encodings can be conceived depending on the choice of $M_{\rm f}$ and $M_{\rm ph}$. When a single frequency carrier is used, $M_{\rm f} = 1$, states differ by only the initial phase; this encoding is known as PSK. When $M_{\rm ph} = 1$, all states differ in frequency; this encoding is known as CFSK. In all other cases, states differ by both frequency and phase, and the encoding is a frequency-phase hybrid (HFPSK). Figure 1 shows constellation diagrams of the modulation-scheme family, and all those modulation schemes are used in this work. Namely, there are four possible encoding schemes with an alphabet length of $M = 8$. Solid circles represent states, whose color represents the frequency, and the angular position of a circle represents the phase shift at the beginning of the pulse. The first constellation corresponds to the CFSK modulation scheme, where all symbols have a different frequency, $M_f = 8$ and $M_{\rm ph} = 1$. The second and third constellations correspond to HFPSK modulation schemes in which states are encoded in four frequencies and two phases, $M_f = 4$ and $M_{\rm ph} = 2$, and two frequencies and four phases, $M_f = 4$ and $M_{\rm ph} = 2$, respectively. The fourth constellation corresponds to PSK, where all states have different phases, $M_f = 8$ and $M_{\rm ph} = 1$.

B. Continuous measurement and the single-shot confidence vector

In a single-shot state-identification problem, we identify an input state $|\psi_s\rangle$ that is randomly chosen among a predefined set of states, $s \in 1, \ldots, M$ (as shown in Fig. 1). To do so, we employ continuous measurement on the input state ψ_s with unknown s over time $t = [0, T]$, where T is the pulse-duration time. We assume the state is in a single spatial mode. The continuous measurement can be written as an operator:

$$\hat{\Omega} = \lim_{dt\to 0} (\hat{C}_T \hat{U}_T \times \cdots \times \hat{C}_{2dt}\hat{U}_{2dt}\hat{C}_{dt}\hat{U}_{dt}),$$

where $\hat{U}$ denotes the coherent displacement operator and $\hat{C}$ denotes photon counting during time dt. We record the measurement history $\mathbb{Z}[0, T] = (\lambda_t, \ldots, \lambda_{2dt}, \lambda_{dt}; \hat{U}_t, \ldots, \hat{U}_{2dt}, \hat{U}_{dt})$ for each period T.

In the limit of weak input, this record contains detection times on a photon-counting detector, whose number cannot be predicted. It also contains information on all displacements applied. The algorithm for selecting displacements depends on the optimization goal for state identification. Here, we are interested in reducing the symbol error rate (SER). To achieve this goal, the state identification is done with a feedback mechanism in which, during the measurement, we use an incomplete detection record $\mathbb{Z}[0,t]$ to guess the most likely input state s' using the Bayes inference $t < T$ [26] and apply the local oscillator (LO) that will displace s' to vacuum. With such an LO, the likelihood that the detector will click is close to zero if $s = s'$ and is nonzero if the guess is incorrect ($s \neq s'$):

$$p(\psi_s|\mathbb{Z}[0,t]) = \frac{p(\mathbb{Z}[0,t]|\psi_s)\tilde{p}_s}{p(\mathbb{Z}[0,t])}. \tag{1}$$

Here, $p(\mathbb{Z}[0,t]|\psi_s)$ is the posterior probability that the measurement record $\mathbb{Z}[0,t]$ occurs if the input state was ψ_s, and $\tilde{p}_s$ is the prior probability. The values of prior probabilities at the beginning of the measurement $t = 0$ are known from the formulation of the problem. After each photon detection, the probabilities are updated. This Bayesian calculation is obtained for all M possible input states, and the resulting posterior probabilities can be expressed as a vector, $\vec{P} = \{p_s\}$, known as a confidence *a posteriori* vector. In our case, it comprises eight probabilities corresponding to $M = 8$ states. The state for displacement s' corresponds to the maximal component of $\vec{P}$. Once the measurement is completed, $t = T$, we calculate the final set of probabilities $p(\psi_s|\mathbb{Z}[0,T])$ to find the final confidence vector $\vec{P}_T$ (also comprising eight probabilities).

In our prior work we showed that, using a continuous measurement on the input state can be advantageous compared to traditional homodyne and heterodyne measurements. A typical metric used to quantify this advantage is a comparison of the state with the highest confidence and the true input state for a large ensemble of measurements. An error occurs when the two are different. The so-called symbol error rate is the ratio of the number of incorrectly identified symbols to the total number of symbols. As we will see, our measurements compare favorably to the ideal symbol error rate of the optimal classical heterodyne measurement. In other words, this rather naive approach to state identification already offers a quantum advantage. In this paper, we show that even more information can be extracted from continuous measurement.

C. Experimental setup

The experimental setup for single-shot confidence estimation is shown in Fig. 2. The same setup is used for all constellations shown in Fig. 1. The only difference is the firmware of the field-programmable gate array (FPGA), which contains constellation-specific instructions to generate states and rules to calculate $p(\mathbb{Z}[0,t]|\psi_s)$. During the single-shot experiment of duration 0 to T ($T = 64$ μs), the input state ψ_s is chosen at random. It is prepared by transmitter Tx and sent to the receiver Rx. The mean photon number of the input state is ≈1 photon/bit after adjusting to the system efficiency. The receiver Rx comprises an LO, a 99:1 unbalanced beam splitter (BS), a superconducting nanowire single-photon detector (SNSPD), and the FPGA. At the Rx, the input signal is combined with the LO on a BS. Both Tx and Rx operate at the telecom wavelength of 1550 nm and are enabled by the same laser. The LO displaces the input signal into the vacuum if the LO hypothesis matches the input state; otherwise, the displacement can lead to photon detection. The output of the BS is fed into the SNSPD, and subsequently, the output of the SNSPD is sent to the FPGA that runs the feedback algorithm. The example in the inset in Fig. 2 shows time-resolved photon detections at the SNSPD during the measurement. Although confidence vectors evolve in time, only photon-detection events lead to the hypothesis change. Thus, after each photon detection t_i, the FPGA recalculates the confidence vector $p(\psi_s|\mathbb{Z}[0,t_i])$ and switches the hypothesis to the state with the highest confidence, given the new information (a click on the detector). At the end of each measurement, its unique measurement history $\mathbb{Z}[0,T]$ is transferred to a personal computer in real time. The adaptive algorithm is described in more detail in the next section.

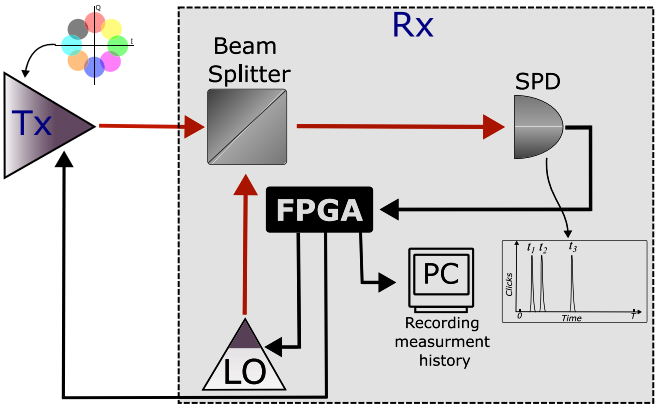

FIG. 2. The test-bed diagram. Transmitter Tx randomly chooses an input signal state from a constellation and sends it to the quantum-enabled receiver for state identification. The receiver Rx comprises the LO, 99:1 BS, an SNSPD, and an FPGA. The FPGA controls the Tx and Rx modules for simplicity of the setup. The FPGA generates rf signals that modulate the Tx light and prepares the LO in the Rx module. It also runs the adaptive Rx algorithm for the LO based on feedback from the SNSPD. The inset shows an example of a signal from a detector, here with three detected photons. The time signatures of photon detections are resolved by the FPGA and used as input for the feedback algorithm. Those time signatures are also stored and transmitted to the PC as part of the measurement record $\mathbb{Z}[0,t]$.

We collect transmitted signals, times of photon detections, displacement operators, and the final confidence vector. This real-time information of each measurement is used for further analysis, statistical verification, and visualization. To obtain relevant ensemble averages (e.g., of successful state identification) we repeat the measurement for all the possible states in the alphabet 50 000 times.

D. The state-identification algorithm

The state-identification algorithm is an adaptive algorithm that changes the LO settings to minimize the probability of

error in identification. Because the input state is chosen at random, we set all M of our prior probabilities to $1/M$, so that $\vec{P}_{t=0} = \{1/M, \ldots, 1/M\}$. Therefore, for $M = 8$, the initial confidence vector is $\vec{P}_{t=0} = \{0.125, \ldots, 0.125\}$. Because all components in $\vec{P}_{t=0}$ are equiprobable, we can set our initial hypothesis to any state without the loss of generality. Here, we begin our identification by setting the hypothesis to be the first state $\psi_{s'=1}$. The LO is set to extinguish the output of a beam splitter to vacuum if $s = s'$.

We monitor and record the time of photoelectronic detections in real time. These data are used to update the Bayesian probabilities at intermediate times $t < T$. It turns out that the hypothesis needs to be adjusted only if a photon detection occurred. This is because the Bayesian probability that the input is in the state identified by a hypothesis monotonically grows in the absence of a photon detection. After each photon detection, we update the confidence vector and choose the hypothesis state with the highest probability s' as the next best guess h_i. The LO is then set to displace the signal according to the hypothesis. To compute probabilities, this algorithm follows the Bayesian inference formula in Eq. (1): it uses the incomplete measurement record $\mathbb{Z}[0, t]$ and calculates the incomplete confidence vector. At the end of the measurement duration T, we obtain the final record of measurement history $\mathbb{Z}[0, T] = (t_1, t_2, \ldots, t_M; \hat{U}_{h_0}, \hat{U}_{h_1}, \ldots, \hat{U}_{h_M})$ and compute the final confidence vector $\vec{P}_T = (p_1, p_2, \ldots, p_M)$.

E. Experimentally obtained measurement records and confidence vectors

In our experiment, we measure and store the measurement record and recover the confidence vector and its evolution in time for each individual measurement. Because photon-detection times are random, both the number of photon detections and the exact times of photon detections are unique for each act of measurement. Owing to this inherent uncertainty, these values are unpredictable, even in principle, before the measurement commences. Examples of typical experimental results for different modulation schemes are shown in Fig. 3. Particularly, there are examples of the measurement records $\mathbb{Z}[0, T]$, which contain photon-detection times and the history of applied displacements for an individual act of measurement. Examples of corresponding confidence vectors and their evolution through continuous measurement are also shown. These values are obtained from Eq. (1). The values of the final confidence vector $\vec{P}_T$ are shown in the graph (at $t = T$) and separately on a pie chart. Note that the components of the vector are discontinuous. As discussed before, each photon detection invalidates the current hypothesis. Therefore, discontinuities occur every time a photon is registered at the output. Figures 3(a)–3(d) show examples of single-shot-measurement confidence estimation for $M_{\text{ph}} = 8$ and $M_{\text{ph}} = 1$, $M_{\text{ph}} = 4$ and $M_{\text{ph}} = 2$, $M_{\text{ph}} = 2$ and $M_{\text{ph}} = 4$, and $M_{\text{ph}} = 1$ and $M_{\text{ph}} = 8$, respectively. For a given Tx, there are eight possible confidence vectors (shown in eight different colors), and its value changes over time. The graph represents the evolution of the state's probabilities for all the states in the constellation with rapid jumps at each photon detection. The eight colors represent the eight states of the alphabet, and the corresponding colors are used in the pie chart to show the final confidence vector (probability distribution). $\mathbb{Z}[0, T]$ contains the information of photon arrival time (scaled to the measurement time T) and chosen displacements. We start with equal probabilities of all states, and the initial hypothesis is $\psi_{s=1}$; hence, the probability of state ψ_1 (black) grows before the first photon detection is registered. After each photon detection, based on the photon arrival time, probability vectors are recalculated, and the state with highest probability is assigned as a new hypothesis and included in the measurement record. At $t = T$ the state with the highest Bayesian probability (the highest element of the confidence vector) is the received state Rx, and all the probabilities in the confidence vector are important, as we will show next. Interestingly, some components of the vector $\vec{P}$ oscillate. This behavior is because we use frequency modulations, and interfering coherent states at different, slightly detuned frequencies result in a temporal fringe in the probability to detect a photon [see Fig. 3(d)], where only one carrier frequency for all states in a constellation is used.

TABLE I. Experimentally obtained SER and the theoretical limit for modulation schemes used in this paper at ≈1 photon/bit. The quantum advantage is the ratio of the experimentally measured SER_{exp} to the theoretical shot-noise-limited SER (SER_{SNL}).

Modulation	SER_{exp} (%)	SER_{SNL} (%)	$\frac{\text{SER}_{\text{exp}}}{\text{SER}_{\text{SNL}}}$ (dB)
$M_f = 8, M_{\text{ph}} = 1$	5.3	14.5	−4.3
$M_f = 4, M_{\text{ph}} = 2$	12.3	15.6	−1.3
$M_f = 2, M_{\text{ph}} = 4$	13.6	14.7	−0.3
$M_f = 1, M_{\text{ph}} = 8$	21.3	34.1	−2.0

We expect that the more "information" is acquired within one measurement, the higher the confidence in the final result will be. Indeed, as is evident from Fig. 3(b), a click is registered at the very beginning of the pulse, and the corresponding hypothesis is tested for a relatively long time; thus, the confidence in the result is high. A similar effect can be seen in Figs. 3(a) and 3(d), where a significant number of photon detections is combined with an appreciable time of the final hypothesis testing. In all the above cases, the largest Bayesian probability is 80% or higher. In contrast, in Fig. 3(c) the last hypothesis is tested only briefly, so there is insufficient time until the end of the measurement to verify it well. As a result, a vector with low confidence values is recorded, and a comparison of the transmitted and received states indicates that the state identification has failed.

F. The physical significance of the confidence vector

If measurement records are not analyzed and only the state with the highest confidence is considered as the identification outcome, one can easily quantify the experimental SER and compare it to the shot-noise limit (SNL) based on all experimental data (a large ensemble). Table I shows the experimentally obtained SER and the corresponding theoretical limit (SNL) at ≈1 photon/bit for each modulation scheme in this paper. As seen from Table I, our quantum receiver operates with quantum advantage.

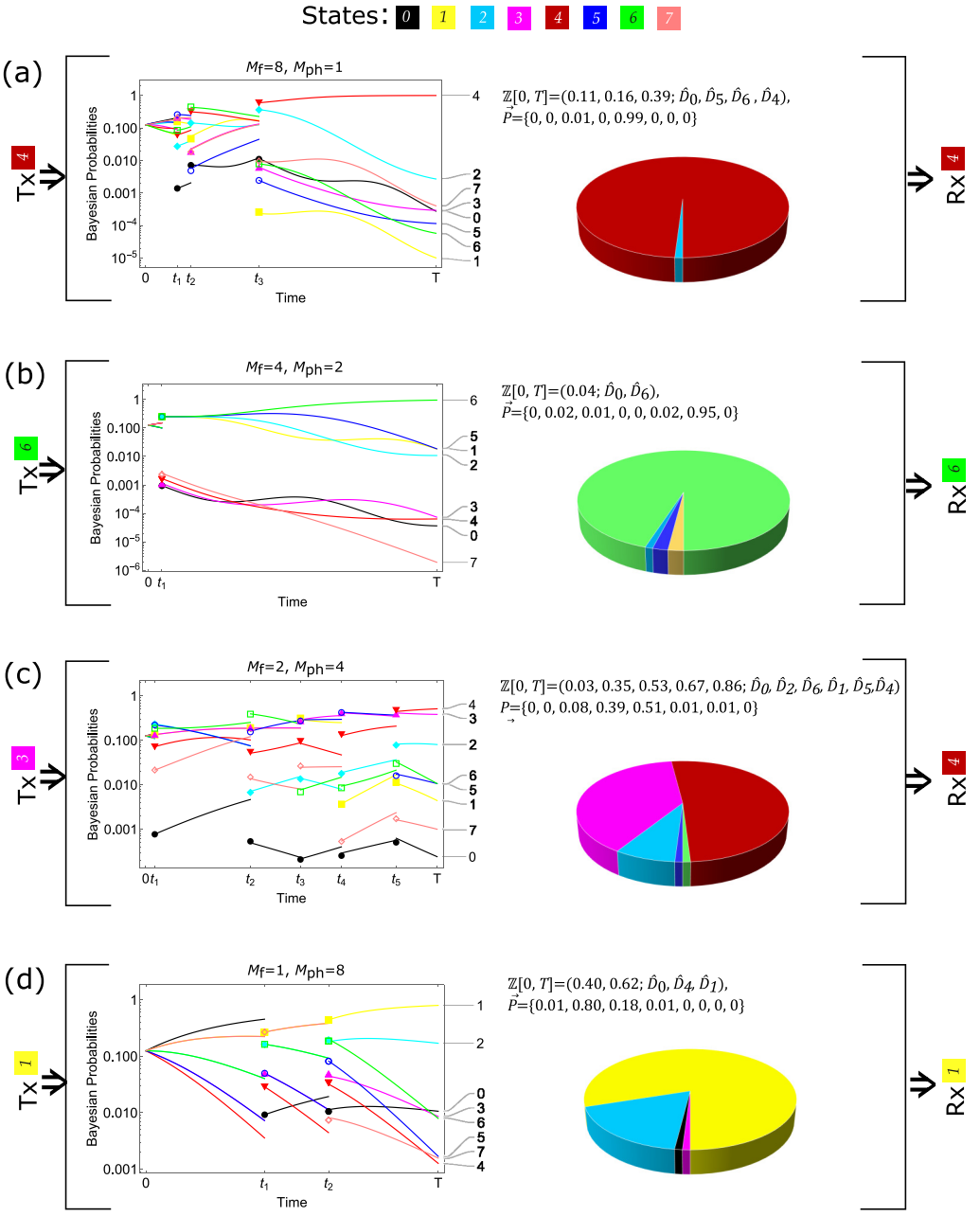

FIG. 3. Examples of the confidence vector during measurement period 0 to T, recorded measurement history $\mathbb{Z}[0, T]$, and confidence vector $\vec{P}$ are shown for different modulations: (a) $M_f = 8, M_{\text{ph}} = 1$, (b) $M_f = 4, M_{\text{ph}} = 2$, (c) $M_f = 2, M_{\text{ph}} = 4$, and (d) $M_f = 1, M_{\text{ph}} = 8$. The input states sent by Tx are shown in different colors and tagged by numbers 0 to 7. The confidence vector $\vec{P}$ obtained at the end of the measurement is depicted in the pie chart. Each graph shows different trends and resolves into unique outcomes. The received state Rx is the state with the highest probability.

Here, we experimentally establish that individual Bayesian estimates, different for each act of measurement, contain even more useful information. Particularly, given the confidence vector, one can predict the reliability of each measurement separately, well beyond the ensemble-averaged benchmarks, such as SER. Indeed, given the above discussion, one expects that irrespective of the magnitude of a confidence value p_s, any sth component of the confidence vector (calculated based on a single measurement record) correlates with the frequentist probability (ensemble-based Kolmogorov probability) that the true input state was s. At issue here is the uniqueness of every measurement record and the need for an ensemble that would allow us to correctly calculate a frequentist probability. To do so, all elements of all collected confidence vectors $\vec{P} = p_0, p_1, \ldots, p_M$ are divided into 10% bins. To find the average value of the Bayesian probabilities in each 10% bin, we calculated the mean values of the confidence vector components that fall into that bin. It turns out that most of those averages are close to the middle of the bin, except in the very first and the very last bins. Indeed, the first average is $\bar{p}_{[0\%,\ldots,10\%]} \approx 0\% \neq 5\%$ for all encodings, and the last average $\bar{p}_{[90\%,\ldots,100\%]} \neq 95\%$ but varies from encod-

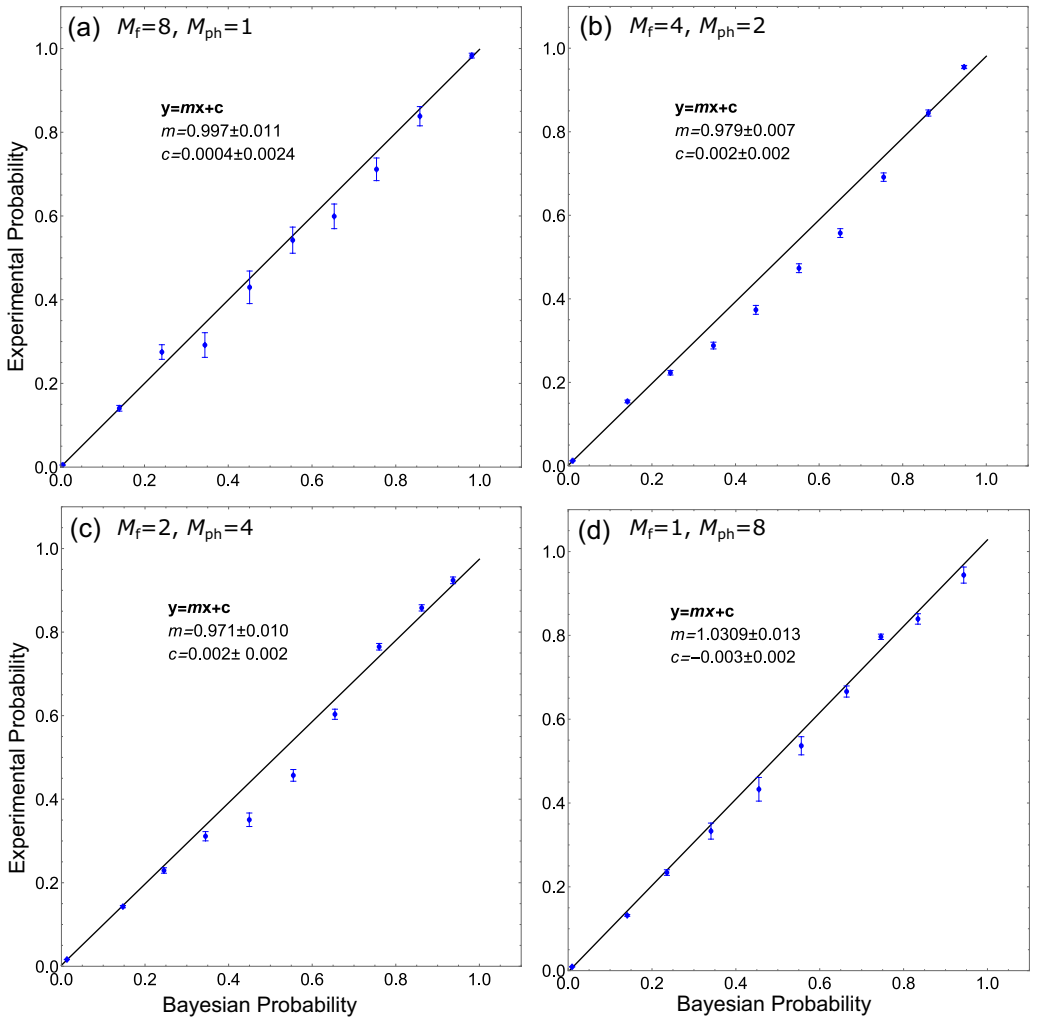

FIG. 4. Experimental evidence of Bayesian probabilities truly represents the best knowledge of the input signal. Experimental probabilities are plotted against the Bayesian probabilities for the modulation scheme: (a) $M_f = 8, M_{\rm ph} = 1$, (b) $M_f = 4, M_{\rm ph} = 2$, (c) $M_f = 2, M_{\rm ph} = 4$, and (d) $M_f = 1, M_{\rm ph} = 8$. Blue dots are experimental results, and black solid lines are linear fits to the experimental data. Error bars show one standard deviation estimated from statistical error.

ing to encoding. This is because our quantum measurement often yields Bayesian probabilities that are close to unity for one of the states, which means that other components of the confidence vector should be close to zero. Thus, we end up with 10 ensembles of Bayesian probabilities with similar values. Now, for each such ensemble, we find the fraction of times the sent state was in a state whose Bayesian probability fell in that ensemble. The experimental ensemble probabilities are $q(p) = N_{\rm correct}/(N_{\rm correct} + N_{\rm incorrect})$, where q is a frequentist probability, p is the average Bayesian probability in the ensemble, and $N_{\rm correct}$ and $N_{\rm incorrect}$ are the numbers of successful and unsuccessful identifications, respectively.

Now, to prove that the Bayesian confidence vector $\vec{P}$ represents the best knowledge about the input state, we experimentally show that the ensemble average of the successful identification of the measured state (a frequentist probability) matches the single-shot probability (Bayesian probabilities), shown in Fig. 4. The x axis represents the average Bayesian probability in 1 of 10 bins, and the y axis represents frequentist (Kolmogorov) probabilities. If, indeed, the confidence vector represents our best knowledge of the input state postmeasurement, the two values should be identical.

Figures 4(a)–4(d) show the Bayesian vs experimental probability for the modulations $M_f = 8$ and $M_{\rm ph} = 1$, $M_f = 4$ and $M_{\rm ph} = 2$, $M_f = 2$ and $M_{\rm ph} = 4$, and $M_f = 1$ and $M_{\rm ph} = 8$, respectively. We see experimentally, irrespective of the modulation scheme, the measured frequentist probabilities of successful identification observed for an ensemble of single-shot measurements q are equal to the observed single-shot confidence estimations p. Interestingly, this is true for any value of p, including for low confidence, $p \approx 0$, and high confidence, $p \approx 1$. In addition, this equality holds for all the modulations we tested in our experiments. To test any deviations from the expected dependence, $q(p) = p$, we use the least-squares method for linear fitting of experimental data, shown as black solid lines in Fig. 4. The linear fitting equation, $y = mx + c$, and corresponding coefficients, slope m and x intercept c, are shown in each plot. The obtained values of m are close to unity, and the x intercepts c are close to zero to within the measurement error. This is true for all modulation schemes tested in the experiment. The unit slope and

zero intercepts confirm that single-shot confidence a posteriori vectors P indeed represent our best knowledge about the measured state and are directly related to the expected frequentist probabilities, calculated from an ensemble of measurements.

III. CONCLUSION

In conclusion, we explored the concept of single-shot continuous measurement where the unknown input state is identified and confidence values associated with each measurement are obtained. We used time-resolved quantum measurement to identify the state to improve the probability of successful identification with SER below the shot-noise limit. Because of the unique features of our method, multiple modulation schemes can be tested without a change in the optical layout. Accordingly, we tested eight states (alphabet length $M = 8$) using four different modulations. We experimentally showed that the ensemble average of the successful identification probability of the measured state matches single-shot Bayesian probabilities; therefore, the Bayesian confidence vector represents our best postmeasurement knowledge about the input state. Remarkably, this is true for all tested modulation schemes. The result indicates that our confidence-estimation algorithm for single-shot estimation is robust and versatile; therefore, it can be used with any desired modulation scheme and alphabet length. In practice, a communication protocol that uses quantum-enhanced receivers can exploit confidence values for quantum-enabled error correction, which can surpass classical detection and error-correcting techniques. Combined with the extremely low energy per bit required for quantum-enabled classical communication, these error-correcting methods suppress the error rate enabling reliable communication. The use of those quantum methods not only enables resource-efficient communications but also can naturally solve the coexistence problem of classical and quantum channels in the same fiber, enabling future blended classical and quantum networks. In addition, this study contributes to advancing the understanding of fundamental properties of quantum measurement and can be thought of as a practical application of the quantum Bayesianist paradigm [28].

[1] A. Peres and W. K. Wootters, Optimal detection of quantum information, Phys. Rev. Lett. **66**, 1119 (1991).

[2] JM Geremia, Distinguishing between optical coherent states with imperfect detection, Phys. Rev. A **70**, 062303 (2004).

[3] J. Bae and L.-C. Kwek, Quantum state discrimination and its applications, J. Phys. A **48**, 083001 (2015).

[4] C. W. Helstrom, Quantum detection and estimation theory, J. Stat. Phys. **1**, 231 (1969).

[5] A. S. Holevo, On the capacity of quantum communication channel, Probl. Peredachi Inform. **15**, 3 (1979) [Problems of Inform. Transm. **15**, 247 (1979)].

[6] S. J. Dolinar, An optimum receiver for the binary coherent state quantum channel, Quarterly Progress Report No. 111 (Research Laboratory of Electronics, M.I.T., 1973), pp. 115–120.

[7] R. S. Kennedy, A near-optimum receiver for the binary coherent state quantum channel, Quarterly Progress Report No. 108 (Research Laboratory of Electronics, M.I.T., 1973), pp. 219–225.

[8] I. A. Burenkov, O. V. Tikhonova, and S. V. Polyakov, Quantum receiver for large alphabet communication, Optica **5**, 227 (2018).

[9] I. A. Burenkov, M. V. Jabir, and S. V. Polyakov, Practical quantum-enhanced receivers for classical communication, AVS Quantum Sci. **3**, 025301 (2021).

[10] M. T. DiMario and F. E. Becerra, Single-shot non-Gaussian measurements for optical phase estimation, Phys. Rev. Lett. **125**, 120505 (2020).

[11] F. Becerra, J. Fan, G. Baumgartner, J. Goldhar, J. Kosloski, and A. Migdall, Experimental demonstration of a receiver beating the standard quantum limit for multiple nonorthogonal state discrimination, Nat. Photonics **7**, 147 (2013).

[12] I. A. Burenkov, M. V. Jabir, A. Battou, and S. V. Polyakov, Time-resolving quantum measurement enables energy-efficient, large-alphabet communication, PRX Quantum **1**, 010308 (2020).

[13] M. V. Jabir, I. A. Burenkov, N. F. R. Annafianto, A. Battou, and S. V. Polyakov, Experimental demonstration of the near-quantum optimal receiver, OSA Continuum **3**, 3324 (2020).

[14] K. Tsujino, D. Fukuda, G. Fujii, S. Inoue, M. Fujiwara, M. Takeoka, and M. Sasaki, Sub-shot-noise-limit discrimination of on-off keyed coherent signals via a quantum receiver with a superconducting transition edge sensor, Opt. Express **18**, 8107 (2010).

[15] S. Guha, J. L. Habif, and M. Takeoka, Approaching Helstrom limits to optical pulse-position demodulation using single photon detection and optical feedback, J. Mod. Opt. **58**, 257 (2011).

[16] K. Tsujino, D. Fukuda, G. Fujii, S. Inoue, M. Fujiwara, M. Takeoka, and M. Sasaki, Quantum receiver beyond the standard quantum limit of coherent optical communication, Phys. Rev. Lett. **106**, 250503 (2011).

[17] K. Kato, M. Osaki, M. Sasaki, and O. Hirota, Quantum detection and mutual information for QAM and PSK signals, IEEE Trans. Commun. **47**, 248 (1999).

[18] Y. Zuo, K. Li, and B. Zhu, 16-QAM quantum receiver with hybrid structure outperforming the standard quantum limit, MATEC Web Conf. **61**, 06008 (2016).

[19] F. Becerra, J. Fan, and A. Migdall, Photon number resolution enables quantum receiver for realistic coherent optical communications, Nat. Photonics **9**, 48 (2015).

[20] M. T. DiMario and F. E. Becerra, Robust measurement for the discrimination of binary coherent states, Phys. Rev. Lett. **121**, 023603 (2018).

[21] M. DiMario, L. Kunz, K. Banaszek, and F. Becerra, Optimized communication strategies with binary coherent states over phase noise channels, npj Quantum Inf. **5**, 65 (2019).

[22] S. Izumi, J. S. Neergaard-Nielsen, and U. L. Andersen, Tomography of a feedback measurement with photon detection, Phys. Rev. Lett. **124**, 070502 (2020).

[23] A. R. Ferdinand, M. T. DiMario, and F. E. Becerra, Multi-state discrimination below the quantum noise limit at the single-photon level, npj Quantum Inf. **3**, 43 (2017).

[24] M. L. Shcherbatenko, M. S. Elezov, G. N. Goltsman, and D. V. Sych, Sub-shot-noise-limited fiber-optic quantum receiver, Phys. Rev. A **101**, 032306 (2020).

[25] M. V. Jabir, N. F. R. Annafianto, I. A. Burenkov, M. Dagenais, A. Battou, and S. V. Polyakov, Versatile quantum-enabled telecom receiver, AVS Quantum Sci. **5**, 015001 (2023).

[26] I. A. Burenkov, N. F. R. Annafianto, M. V. Jabir, M. Wayne, A. Battou, and S. V. Polyakov, Experimental shot-by-shot estimation of quantum measurement confidence, Phys. Rev. Lett. **128**, 040404 (2022).

[27] I. A. Burenkov, N. F. R. Annafianto, M. V. Jabir, A. Battou, and S. V. Polyakov, Suppressing communication errors using quantum-enabled forward error correction, AVS Quantum Sci. **5**, 031403 (2023).

[28] C. A. Fuchs, Qbism, the perimeter of quantum Bayesianism, arXiv:1003.5209.

[29] M. V. Jabir, N. F. R. Annafianto, I. A. Burenkov, A. Battou, and S. V. Polyakov, Energy and bandwidth efficiency optimization of quantum-enabled optical communication channels, npj Quantum Inf. **8**, 63 (2022).